ERROR ANALYSIS ON DEMS DETERMINED BY NASA/JPL AIRSAR IN CHINA TAIPEI

Jaan-Rong TSAY*
Ji-Gang Lin**

*Assistant Professor
Department of Surveying Engineering
National Cheng Kung University
1, University Road, 70101 Tainan
Tel: (886)-6-237-0876 ext. 838 Fax: (886)-6-237-5764
E-mail: tsayjr@mail.ncku.edu.tw
CHINA TAIPEI, R.O.C.

**Graduate Student,
Department of Surveying Engineering
National Cheng Kung University
1, University Road, 70101 Tainan
Tel: (886)-6-237-0876 ext. 838 Fax: (886)-6-237-5764
CHINA TAIPEI, R.O.C

KEY WORDS: AIRSAR, TOPSAR, InSAR, DEM, image

ABSTRACT: In this paper, the DEMs determined by airborne InSAR technique (AIRSAR) in the midChina Taipei area during the PacRim 2000 Mission of NASA/JPL are compared with the reference DEMs determined by aerial photogrammetry. The error analysis is done. After horizontal and vertical datum transformation operations, the systematic bias, random error, and blunder as well are estimated and analyzed. Also, the areas where AIRSAR cannot determine the ground surface height are analyzed.

1. INTRODUCTION

Radargrammetry has dramatically progressed and seen great activity in the past decades. Weather independence and 24-hour operation capabilities are two most widely touted and valuable characteristics of radar (=RAdio Detection And Ranging). In the meanwhile, two well-known Synthetic Aperture Radar (SAR) techniques emerged during this time. Polarimetric SARs (POLSAR) were firstly demonstrated during the 1980's and described by (Van Zyl et al, 1987) and (Zebker et al., 1987). Since then POLSAR data have been utilized in the diverse fields of Earth Science. The second powerful SAR technique is Interferometric SAR (InSAR) that was firstly published by (Graham, 1974). The InSAR using digital processing is firstly demonstrated in (Zebker & Goldstein, 1986), and since then interest in InSAR has steadily increased.

2. NASA/JPL AIRSAR/TOPSAR SYSTEM

In this paper, the digital terrain models (DEMs) in China Taipei derived from the NSAR/JPL*airborne* InSAR (AIRSAR) system are to be studied. The NASA/JPL AIRSAR/TOPSAR system can simultaneously acquire inteferometric (C- and/or L-band) and polarimetric data (C-, L- and P-band). The approach to process data acquired in these modes differs from that described by (Madsen et al., 1993) in both the *motion compensation approach*, as well as in the sense that data are*deskew*ed before interferograms are formed. For more detailed information of this processing approach, please see (Van Zyl et al., 2002).

The NASA/JPL AIRSAR system is a three-frequency airborne SAR system and is flown on a NASA DC-8 passenger jet. In 1990 NASA, in collaboration with an Italian consortium (CORISTA), approved the addition of another set of C-band antennas to implement a single-pass, fixed baseline cross-track interferometer (XTI) for topographic mapping. The C-band antennas were provided by CORISTA, while NASA sponsored the system modifications and processor development described by (Madsen et al., 1993). This mode of the AIRSAR system became known as TOPSAR (Zebker et al., 1992) and data have been

acquired since 1991. In 1995 TOPSAR was extended to acquire XTI data simultaneously at C- and L-band (Van Zyl. et al., 1995). All TOPSAR interferometers can be operated in single or dual baseline modes. For *single baseline operation* signals are transmitted out of one antenna only, and the received signals are measured simultaneously through two antennas. In the *dual baseline mode*, signals are alternatively transmitted out of the antennas at either end of the baseline, while the received signals are measured simultaneously through both antennas.

The performance of the TOPSAR instrument and processor was previously reported by (Madsen et al., 1993), who compared the radar derived DEMs with ones derived using conventional optical stereo techniques. Their analysis showed the difference between the DEMs to be 2.2m RMS (=root mean square) in relatively flat terrain, and up to 5.0m in mountainous areas. (Van Zyl et al., 2002) compares the results of their integrated multi-frequency polarimetric and interferometric SAR processor to that of the TOPSAR processor described by (Madsen et al., 1993). They confirm that results for relatively flat areas are typically better than those for high relief areas. Their results of the relative geometry test shows the RMS difference to be 1.3m~2.1m in a flat area covering the Bolivar peninsula near Galveston, Texas, where the total relief is less than 50m, and 2.3m~4.9m in a mountainous area covering part of Mount Rainier in Washington State, where the total relief is about 1500m.

3. TEST DATA

Now, this paper will briefly show and analyze the results of DEMs derived from NASA/JPL TOPSAR as an independent assessment of the height accuracy of the AIRSAR data in China Taipei. The NASA/JPL AIRSAR system acquired the SAR data in China Taipei on the 27th September 2000 during the PacRim 2000 Mission. The data types contain TOPSAR (in Central China Taipei and Ken_Ting China Taipei), POLSAR (in South China Taipei and West China Taipei), and ATI2 (in South China Taipei), where ATI denotes Along Track Interferometry collected at C- and L-band. The National Cheng Kung University (NCKU) purchased some TOPSAR data directly from the CSRSR (=Center for Space and Remote Sensing Research), National Central University, China Taipei. Our integrated TOPSAR data contain DEM, correlation map, incidence map, and C-band VV data. For more details of these data's specification and radar parameters, please see http://airsar.jpl.nasa.gov/documents/genairsar/airsar_paper1.pdf.

Figure 1 shows our seven test areas A~G with XTI1 and XTI2 mode data, respectively. All data of both modes are acquired at different time, but on the same day (27th September 2000). The DEMs in the XTI1 areas are derived from the C-band data, where only the area B contains two data sets, namely B1 and B2. They might be processed by NASA/JPL using different processors or acquired at different time. Dr. Bruce Chapman of the Radar Science and Engineering Section, NASA/JPL, assume that they both meet the AIRSAR specification and suggest us to assess that for them as an independent assessment of the height accuracy of the AIRSAR data. The DEMs in the XTI2 areas F and G are derived from the C- and L-band data, respectively.

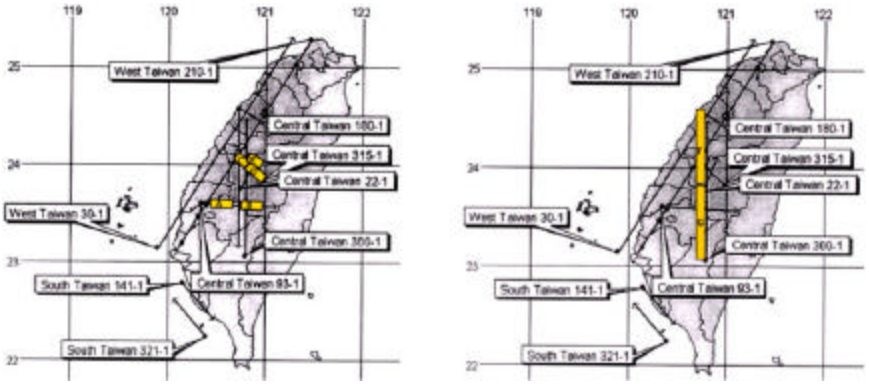

Figure 1 Test areas with XTI1 (left) and XTI2 (right) mode data, where the flight lines are also shown.

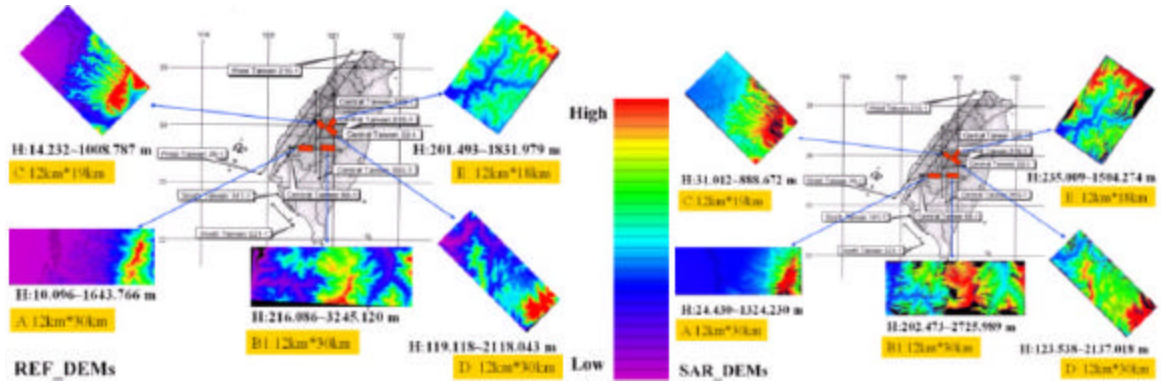

Figure 2 Reference DEMs (left) and DEMs derived from the XTI1 mode data (C-band) (right), where 12km*30km denotes the area of a DEM and H:24.430~1324.230m denotes the range of InSAR-determined height values.

4. RESULTS AND ANALYSIS

All DEMs determined by airborne InSAR technique (AIRSAR), denoted by SAR_DEMs, are computed and provided by NASA/JPL. These DEMs are compared with reference DEMs, denoted by REF_DEMs, determined by aerial photogrammetry. Figures 2 and 3 show both REF_DEMs and their corresponding SAR_DEMs in XTI1 and XTI2 mode, respectively. In general, these test results indicate that both SAR_DEMs and REF_DEMs have very similar terrain surface trend.

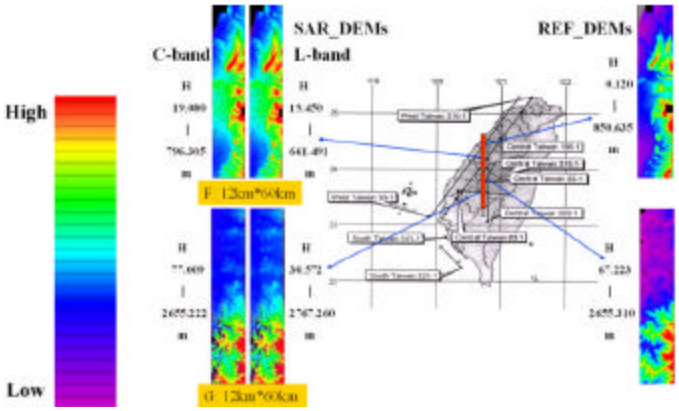

Figure 3 Reference DEMs (right) and DEMs derived from the XTI2 mode data (C- and L-band, left).

4.1 Profile Analysis

Figures 4 and 5 show e.g. two profiles AA' and BB' of SAR_DEM and REF_DEM in the study window A (XTI1 mode) and G (XTI2 mode), respectively. Apparently, significant systematic bias, random errors, and blunders are involved in SAR_DEMs. Also, the results in relatively flat areas are better.

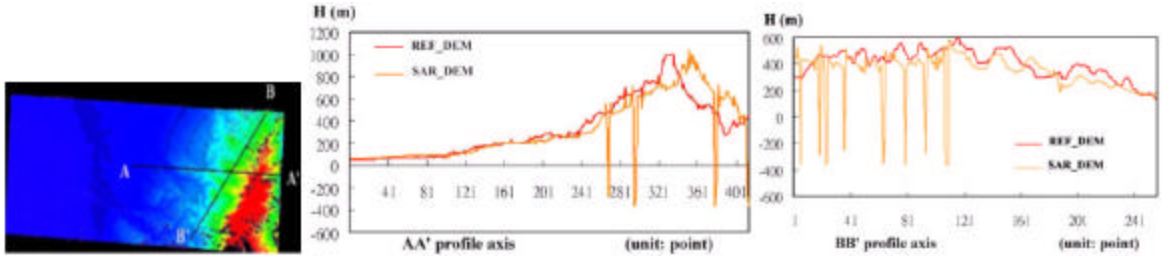

F

Figure 4 Two profiles AA' and BB' of SAR_DEM and REF_DEM in the study window A (XTI1 mode).

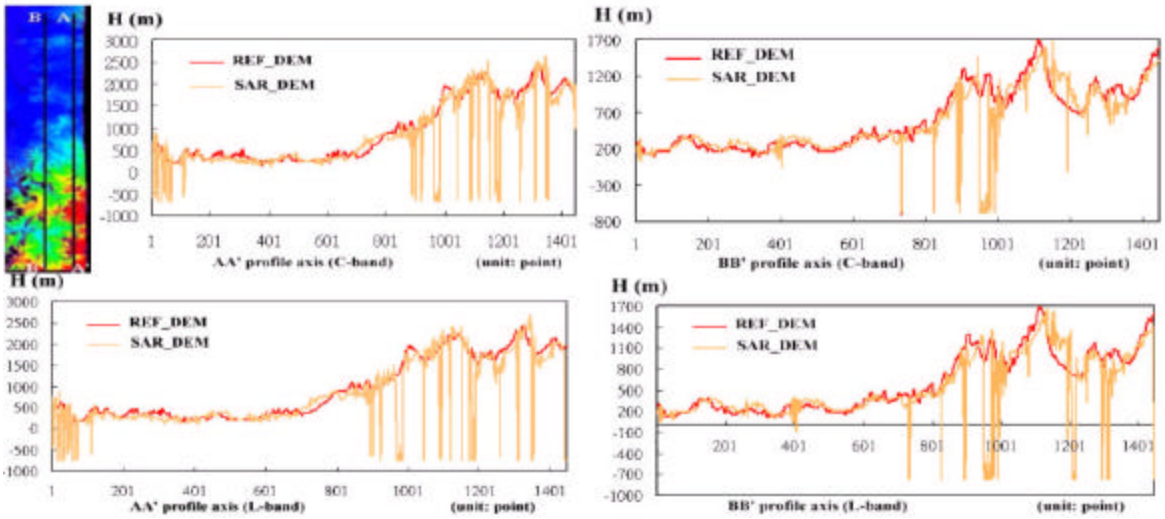

Figure 5 Two profiles AA' and BB' of SAR_DEM and REF_DEM in the study window G (XTI2 mode).

4.2 Height Difference between REF_DEM and SAR_DEM

After horizontal and vertical datum transformation operations, height difference dH is computed on each DEM point by SAR_DEM – REF_DEM. Systematic component in a dH-value, denoted by dH_s, is estimated by a 3x3 mean filter. The random component of dH, denoted by dH_r, is then estimated by dH_r = dH – dH_s. Figure 6 shows a 8-bits coded image that presents the estimated dH_s in the area A, where all values of dH_s are coded with the gray values 50 ≤ G ≤ 220 and all black points (G=0) denote the points, on which AIRSAR cannot determine height values or the related reference height values are not available. The estimated function of dH_s is non-linear in the entire area, though it seems linear or constant in a local window. Table 1 shows clearly that the relative geometry accuracy in flat areas (c.a. 1.3m) is better than that in mountainous areas (c.a. 10.1m). Figure 7 shows that the estimated values of dH_r have approximately the property of Gaussian stochastic error. It also shows the relative accuracy of SAR_DEM in flat areas is better. Table 2 and Figure 8 show the similar results in the window E (mountainous area), where AIRSAR determines a DEM with a relative terrain surface accuracy of c.a. 12.9m.

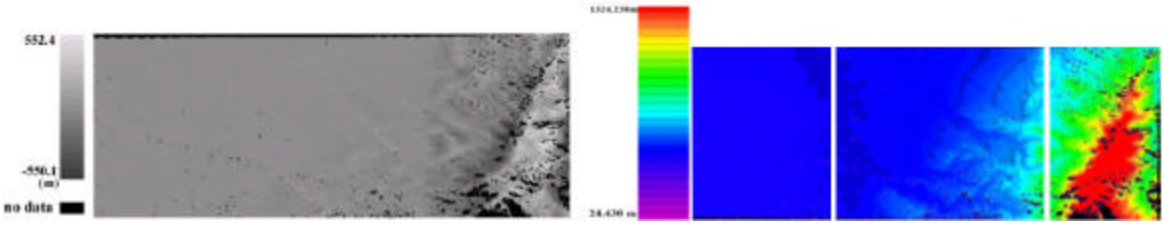

(a) (b)

Figure 6 (a) a 8-bits coded dH_s image in the area A (For detailed description please see the text), (b) Flat area (left) and hilly area (right) in the SAR_DEM window A

Table 1. Statistic figures of estimated systematic and random components of all dH-values in SAR_DEM window A (c.a. 60% flat area, 40% hilly area).

Systematic component dH_s					
	Number of dH-points	Mean (m)	RMS (m)	Min (m)	Max (m)
Entire area	206308	8.24	83.86	-550.14	552.40
Flat area	76272	18.06	18.65	-12.62	37.25
Hilly area	41814	2.23	174.95	-550.14	552.40

Random component dH_r					
	Number of dH-points	Mean (m)	RMS (m)	Min (m)	Max (m)
Entire area	206308	0.00	5.40	-87.19	163.72
Flat area	76272	0.00	1.26	-18.57	40.66
Hilly area	41814	-0.02	10.07	-87.19	163.72

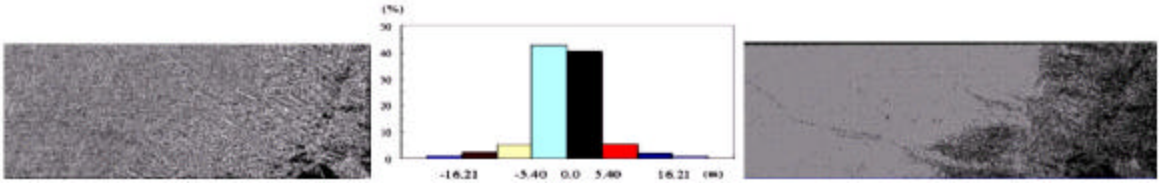

Figure 7 Sign-coded image (left) and histogram (middle) of all estimated random components in the SAR_DEM window A; (right) gray pixels show the points with |dH_r|❍RMS(dH_r)=5.40m in the SAR_DEM window A.

Table 2. Statistic figures of estimated systematic and random components of all dH-values in SAR_DEM window E (hilly area).

Number of dH-points = 99350				
	Mean (m)	RMS (m)	Min (m)	Max (m)
Systematic component dH_s	30.50	143.97	-464.32	533.92
Random component dH_r	0.01	12.89	-188.46	262.62

4.3 Blunder Points in SAR_DEMs

Table 3 shows that there is about 1~2% of DEM points with blunder. Figures 9 and 10 show some examples for illustrating where the blunder points often emerge.

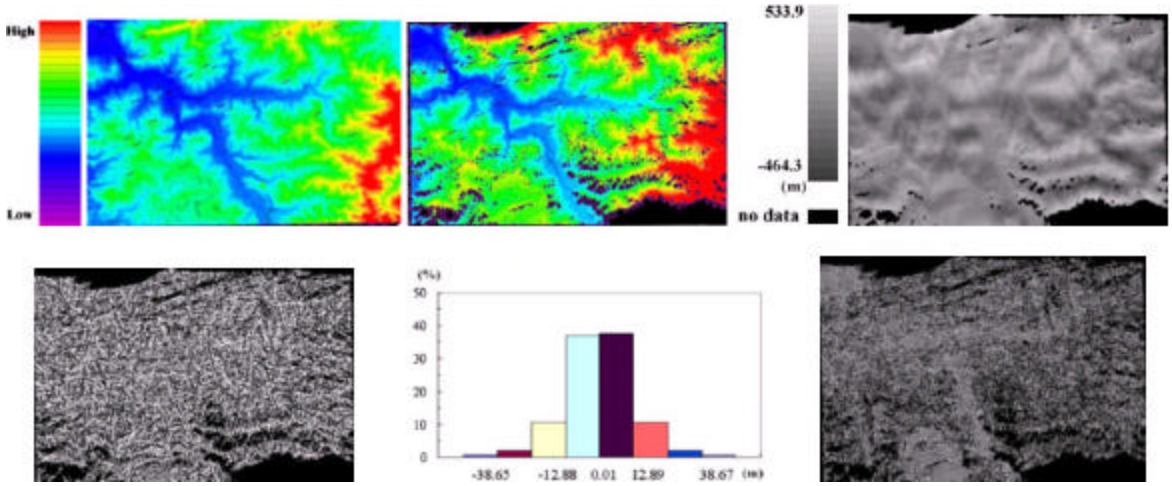

Figure 8 REF_DEM (upper left), SAR_DEM (upper middle), dH_s (upper right), sign-coded image (lower left) and histogram (lower middle) of dH_r, and points with |dH_r|❍RMS(dH_r)=12.89m (lower right) in the window E (hilly area).

Table 3. Statistic figures of blunder points with |dH_r - m|>3RMS(dH_r) in the windows A and E (XTI1 mode) and F and G (XTI2 mode), where m denotes the mean of all dH_r values in a 5x5 window centered at the computed point, RMS(dH_r) is the root mean square value of all dH_r values in a SAR_DEM.

	A	E	F (C-band)	F (L-band)	G (C-band)	G (L-band)
Type of topology	60% flat, 40% hilly	hilly	flat		40% flat, 60% hilly	
No of points	214155	121610	434834	422909	449118	443183
No of blunder points	4119	859	5228	4200	4527	5093
% of blunder points	1.92	0.71	1.20	0.99	1.01	1.15

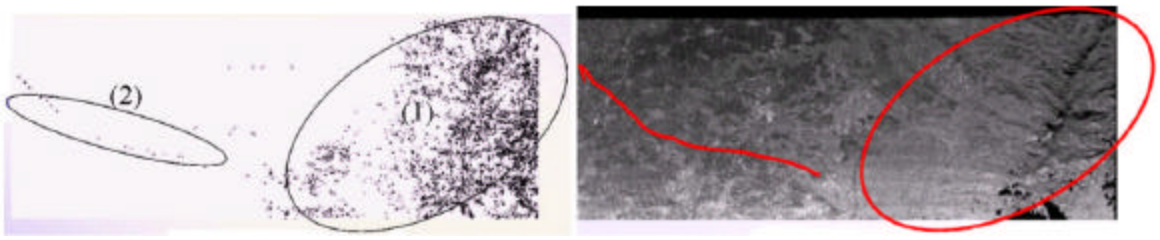

Figure 9 Black points (left) denote blunder points, where the point cloud (1) is in a hilly area and cloud (2) is located on a ditch in a flat area; the power SAR-image of 6095x2405 pixels in the study window A is shown on the right.

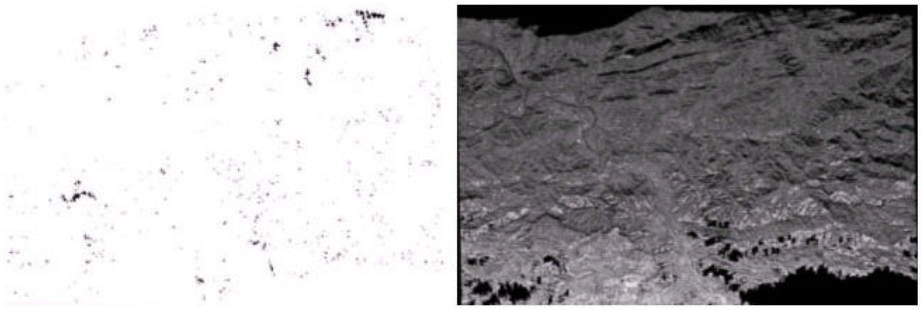

Figure 10 Black points (left) denote blunder points which are located in the shadow areas; the power image of 3606x2403 pixels in the study area E is shown on the right.

4.4 Undeterminable Points in SAR_DEMs

Table 4 shows that the percentage of points, on which AIRSAR cannot determine the heights, is about 6.3% in average and 18.22% in mountainous area, respectively. For instance, a fish pond as shown in Figure 11 is an area where AIRSAR cannot determine the surface height.

Table 4. Statistic figures of the undeterminable points on which airborne InSAR cannot determine the height value in the windows A and E (XTI1 mode) and F and G (XTI2 mode).

	A	E	F (C-band)	F (L-band)	G (C-band)	G (L-band)
Type of topology	60% flat, 40% hilly	hilly	flat		40% flat, 60% hilly	
No of points	214155	121610	434834	422909	449118	443183
No of undeterm. points	7423	22162	10528	9766	37636	36504
% of undeterm. points	3.47	18.22	2.42	2.31	8.38	8.24

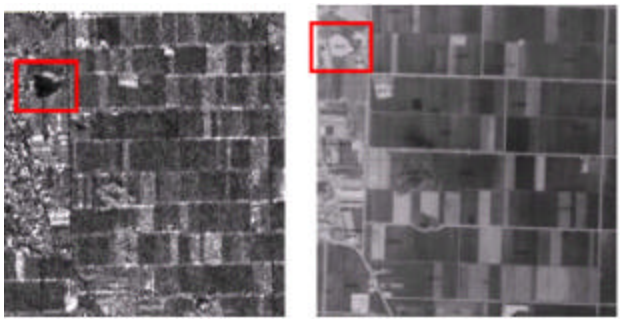

(a) SAR image of 216x233 pixels (b) aerial image of 1524x1572 pixels

Figure 11 An example of undeterminable point area which is a fish pond shown in the red rectangle.

5. CONCLUSION

Our test results indicate that both AIRSAR-determined DEM and reference DEM have very similar terrain surface trend. However, height differences between both still have significant systematic bias, random error, and blunder. The systematic bias is a non-linear function of point position. NASA/JPL AIRSAR determined DEMs in China Taipei have a relative terrain surface accuracy of about 1~2m in flat areas and 10~13m in mountainous areas. In c.a. 2016 km^2 of test areas with about 1.2 million DEM points, there is about 1~2% of SAR_DEM points with blunder. The percentage of points on which AIRSAR cannot determine the heights is about 6% in average and 18% in mountainous areas, respectively. Moreover, efficient techniques in practice for removing systematic errors and reducing stochastic errors in DEMs determined by airborne InSAR on a real terrain such as in China Taipei will and should be further studied.

6. REFERENCES

Graham, L.C., 1974. Synthetic Interferometer Radar for Topographic Mapping. *Proc. IEEE*, Vol. 62, pp. 763-768.

Madsen, S.N., Zebker, H.A., and Martin, J., 1993. Topographic Mapping Using Radar Interferometry: Processing Techniques. *IEEE Trans. Geosci. Remote Sens*., GRS-31, pp. 246-256.

Van Zyl, J.J., Zebker, H.A., and Elachi, C., 1987. Imaging radar polarization signatures: Theory and observation. *Radio Science*, Vol. 22, pp. 529-543.

Van Zyl, J.J., Chu, A., Hensley, S., Lou, Y., Kim, Y., and Madsen, S.N., 2002. The AIRSAR/TOPSAR Integrated Multi-Frequency Polarimerimetric and Interferometric SAR Processor. From http://airsar.jpl.nasa.gov.

Van Zyl, J.J., Zebker, H.A., Hensley, S., and Haub, D.R., 1995. The new dual frequency (C- and L-band) TOPSAR airborne inteferometric SAR. *Proceedings of IGARSS'95*, Florence, Italy, July 10-14.

Zebker, H.A., and Goldstein, R., 1986. Topographic Mapping from Interferometric SAR Observations. *J. Geophys. Res*., Vol. 91, pp. 4993-4999.

Zebker, H.A., Van Zyl, J.J., and Held, D.N., 1987. Imaging radar polarimetry from wave synthesis. *Journal of Geophysical Research*, Vol. 92, No. B1, pp. 683-701.

Zebker, H.A., Madsen, S.N., Martin, J., Wheeler, K.B., Miller, T., Lou, Y., Alberti, G., Vetrella, S., and Cucci, A., 1992. The TOPSAR interferometric Radar Topographic Mapping Instrument. *IEEE Trans. Geosci. Remote Sens*., GRS-30, pp. 933-940.

ACKNOWLEDGEMENT

I greatly appreciate the NSC (=National Science Committee), China Taipei, R.O.C., for sponsoring this work under the research project NSC 91-2211-E-006-112.